Bull. Chem. Soc. Ethiop. **2025**, 39(1), 141-152.
DOI: https://dx.doi.org/10.4314/bcse.v39i1.12

ISSN 1011-3924
Printed in Ethiopia
Online ISSN 1726-801X

PREPARATION OF FLOWER-LIKE HIERARCHICAL STRUCTURE SnO_2/g-C_3N_4 AND ITS ETHANOL GAS-SENSITIVE PROPERTIES

Xiao-Dong Li* and Jia-Wen Pang

Department of Basic Science, Jilin Jianzhu University, 5088 Xincheng Street, Changchun 130118, Jilin Province, China

(Received April 16, 2024; Received in revised July 26, 2024; Accepted September 18, 2024)

ABSTRACT. The flower-like hierarchical structured SnO_2/g-C_3N_4 nanocomposites were successfully prepared by one-step hydrothermal method with high-temperature calcination. The structure and morphology of the synthesized samples were characterized by X-ray powder diffraction (XRD), scanning electron microscopy (SEM) and N_2 adsorption-desorption. The gas-sensitive performance of the pure SnO_2 and SnO_2/g-C_3N_4 sensors were investigated and compared towards ethanol gas. The results showed that the response of the SnO_2/g-C_3N_4 composites to 100 ppm ethanol gas at 200 °C was 18.88, which was 2.09 times that of pure SnO_2, with response and recovery time of 2 s and 13 s. In addition, the gas sensor has excellent selectivity for ethanol gas, good repeatability, and long-term stability. These gas-sensitive properties of the flower-like graded structure SnO_2/g-C_3N_4 to ethanol gas are attributed to the materials which have unique graded structure and n-n heterojunction.

KEY WORDS: Hierarchical structure, SnO_2/g-C_3N_4, Gas sensing property

INTRODUCTION

Graphite like carbon nitride (g-C_3N_4) is a typical polymer semiconductor material with a planar two-dimensional layered structure in its spatial configuration. Usually, there are two types of structures, one is the triazine ring (C_3N_3) and the other is the tris-triazine ring (C_6N_7), with interlayer bonding through van der Waals forces. The CN atoms in both structures are hybridized with sp^2 to form highly delocalized π conjugated systems, resulting in excellent physicochemical properties. For example, good chemical stability can maintain performance stability even in strong acids and alkalis; good thermal stability, able to maintain its working performance at a high temperature of 600 ℃. Easy to prepare and pollution-free, it is a good environmentally friendly material. Recently, many researchers have devoted themselves to the research of ethanol gas sensors. Among the many metal oxide semiconductors, SnO_2 has become one of the most widely used metal oxide semiconductors due to the advantages of its high electron mobility and simple preparation method. Current preparation methods for SnO_2 are relatively mature, including hydrothermal method [1], sol-gel method [2], biotemplate synthesis method [3], and electrostatic spinning techniques [4], which are useful for producing SnO_2 nanomaterials with different properties under different conditions. However, there are many drawbacks which prevent the direct application of the metal oxide semiconductors, such as low gas response, high operating temperature, and poor selectivity. Therefore, metal oxide semiconductors need to be modified to improve their gas-sensitive performance.

The preparation of SnO_2 micro-nanostructure with controllable size and morphology is the effective approach, such as 0D nanoparticles [5], 1D nanorods [6], nanowires [7], nanofibers [8], 2D nanosheets [9], and 3D hierarchical structures [10, 11]. Among them, the 3D hierarchical structure is assembled from low-dimensional nanomaterials, which not only can overcome the disadvantages of low-dimensional materials such as agglomeration and instability but also can provide many oxygen adsorption sites to promote efficient gas diffusion, and enhance gas response. For example, Wang *et al.* [12] prepared hierarchically structured SnO_2 nanoflowers

*Corresponding authors. E-mail: lxdjlju@163.com

assembled by nanorods using a template-free hydrothermal method. Gas sensing studies showed that the SnO_2 nanoflowers have high response and fast response recovery capabilities and are capable of detecting acetone and ethanol at operating temperature below 200 °C. Hu et al. [13] prepared nanosheets and assembled hierarchically structured SnO_2 nanoflowers by a simple hydrothermal method, which showed a response of 34.6 to 100 ppm formaldehyde at 300 °C and exhibited excellent selectivity for formaldehyde gas. Another approach to modify properties is the creation of SnO_2-based composites, which includes doping noble metals and creating heterogeneous structures. The sensitization of noble metals and the interaction of hetero-structures are effective methods to improve the gas-sensitive performance. Zhang *et al.* [14] produced graded porous fish-scale Ag/SnO_2 composites using a straightforward two-step technique with strong selectivity for triethylamine gas and high responsiveness at a low operating temperature of 170 °C. By using a hydrothermal process, Fan *et al.* [15] created 3D nanostructured Pt/SnO_2 composites that responded to 100 ppm ethanol 2.5 times faster than pure SnO_2 nanosheets at 240 °C and recovered more quickly. By using a one-step hydrothermal process, Xue *et al.* [16] created heterojunctional CeO_2/SnO_2 composites that resembled flowers. The results showed that compared with pure SnO_2, the CeO_2/SnO_2 composite displayed much improved gas-sensitive characteristics to triethylamine, and its selectivity was also significantly better. The development of n-n heterojunctions between CeO_2 and SnO_2 led to the composites' improved gas-sensitive properties. By using a two-step hydrothermal method, Liu *et al.* [17] created a novel graded SnO_2 nanorod/spun filamentary α-Fe_2O_3 hetero-structure. As a result of the synergistic interaction between the hetero-structure and the material interfaces, the composite exhibited excellent acetone gas-sensitive properties. However, extensive works have been done on how to improve the performance of gas sensing materials. Due to the unique properties of the g-C_3N_4, it has widely used in various application fields such as photocatalyst, sensors, solar cell and catalysts.

Ethanol (C_2H_6O), commonly known as alcohol, is a type of alcohol compound and a common volatile organic compound. Under normal temperature and pressure, it is a colorless transparent liquid that is flammable, volatile, and easily diffused. It has a pungent odor and can be miscible with water in any proportion or with most organic solvents. Due to its unique properties and relatively low manufacturing costs, it is widely used in the chemical industry, medical and health fields, such as fuel preparation, medical alcohol, beverages, etc. But it has a certain degree of toxicity, which can harm the nervous system after entering the human body, and in severe cases, it can cause poisoning, which is very harmful to human health. In addition, the mixture of ethanol vapor and air can form explosive mixtures, which can easily cause fire and other hazards, in specific occasions, such as distilleries, it is necessary to detect the concentration of ethanol in the air to avoid explosions and fires. In the current research, we attempted to create SnO_2/g-C_3N_4 composites with a graded structure resembling flowers using a one-step hydrothermal process, followed by high-temperature calcination. The unique morphology can provide large contact area and short diffusion length for ionic and electronic transport, so that the kinetics of the reaction is effectively improved. The gas-sensitive property SnO_2/g-C_3N_4 to ethanol will be tested and the gas sensitivity mechanism will be explored. The improved gas sensing properties to ethanol could be due to the higher surface accessibility and reduced the band gap width of the material. Moreover, the possible interactions between SnO_2 and g-C_3N_4 could be also advantageous to improve gas sensing performance.

EXPERIMENTAL

The experimental materials were all analytical grade and commercially available. Thiourea was the raw material for the preparation of block shaped g-C_3N_4 by thermal polymerization, then g-C_3N_4 nanosheets were created through liquid exfoliation assisted by ultrasound method. The specific experimental steps as following: firstly, the weighted thiourea was put in an alumina crucible with a lid and heated to 550 °C for three hours in a muffle furnace to produce yellow block shaped g-C_3N_4. Secondly, liquid exfoliation assisted by ultrasonic was used to exfoliate the

prepared block shaped g-C_3N_4 to layered g-C_3N_4 nanosheets. 5 g block shaped g-C_3N_4 was put into 30 mL isopropanol solution then sonicated mixture 30 h. The color of g-C_3N_4 under sonication was transformed from yellow to light yellow, which means the block shaped material had been completely exfoliated to nanosheets. Finally, in order to get dry powder, the suspension was put in a surface dish and kept in an oven at 60 °C for several hours.

Firstly, 5 mmol $SnCl_2 \cdot 2H_2O$ and 10 mmol $Na_3C_6H_5O_7 \cdot 2H_2O$ were added into 40 mL mixed solution of anhydrous ethanol and deionized water (1:1 ratio) and stirred continuously for 1 h. Then, 2.5 mmol of NaOH was added, and the mixture was stirred for an additional 1 h. Next, a specific quantity of g-C_3N_4 were added, stirred for 15 min, and sonicated for 15 min. After sonication, the mixture was transferred to a 50-mL autoclave lined with PTFE and heated to 180 °C for 12 h in an oven to complete the reaction. The supernatant was removed after the reaction, and the precipitate was collected using a centrifuge tube and rinsed three times with deionized water and anhydrous ethanol. The autoclave was then cooled to room temperature. The cleaned item was dried in the oven at 60 °C the whole night. Finally, the material is calcined at 500 °C for 2 hours to get the final product. SnO_2 composites with 2.5, 5, and 7.5 wt% g-C_3N_4 doped were made by adjusting the addition amount of g-C_3N_4 that are designated as SnO_2/g-C_3N_4-2.5, SnO_2/g-C_3N_4-5, and SnO_2/g-C_3N_4-7.5. For comparison, pure SnO_2 was generated under identical conditions with the exception of the absence of g-C_3N_4.

The physical composition and crystal structure of the samples were measured using an Ultima IV X-ray diffractometer (XRD) from Riguka, Japan, with the scanning angle of 20°-80° and the scanning rate of 5°/min. The morphology and microscopic surface morphology of the materials were observed using an S-4800 scanning electron microscope (SEM) from Hitachi, Japan. The composition and chemical elements of the samples were analyzed by energy dispersive spectroscopy (EDS). The specific surface area was calculated on an Autosorb iQ N_2 adsorption-desorption instrument using the Brunauer-Emmett-Teller (BET) method.

Preparation of sensor components for synthetic samples. First of all, a small amount of prepared sample is placed in an agate mortar with a mixture of deionized water and anhydrous ethanol (the ratio is 9:1) and ground to form a paste-like slurry, then the slurry was evenly coated with a brush on an alumina ceramic pavilion (size about 2.5 × 4.0 nm) to form a uniform film. The ceramic tube contains a pair of gold electrodes and two platinum wires at each end. The ceramic tubes coated with the material slurry were dried in an infrared drying oven until the slurry was cured, and then sintered at 500 °C for 2 h until the deionized water and anhydrous ethanol has completely evaporated. Following this, the Ni-Cr alloy coil was inserted into the tube as a heater, and the ceramic tube was welded to the base with six probes. To improve the stability of the gas sensor and the repeatability of the test, the soldered sensor element was placed on an aging table and aged at a temperature of 200 °C for 48 h. Eventually, a gas sensitivity test was performed on a CGS-8 intelligent gas analysis system. In this task, the sensor response (S) was defined as Ra/Rg, where Ra and Rg denote the resistance values of the sensor in air and target gas, respectively. The response and recovery times are defined as the time required to reach 90% of the total resistance change in the case of adsorption and desorption (referring to the target gas), respectively.

RESULTS AND DISCUSSION

X-ray diffraction (XRD) analysis

XRD patterns were used to examine the materials' crystal structure and physical phase composition. The XRD patterns of g-C_3N_4, SnO_2 and SnO_2/g-C_3N_4 composites are displayed in Figure 1. The g-C_3N_4 curve exhibits a distinctive peak around 27.5°, which corresponds to the compound's (002) crystal plane [18]. All diffraction peaks of SnO_2 and SnO_2/g-C_3N_4 composites correspond to SnO_2 with tetragonal rutile structure (JCPDS Card No. 41-1445), and three major diffraction peaks can be found at $2\theta \sim 26.6°$, 33.9° and 51.8°, respectively, corresponding to (110),

(101) and (211) of the SnO_2 crystal crystalline planes. The intensity of the characteristic peaks in the SnO_2/g-C_3N_4 composite is higher than that of pure SnO_2, indicating that the doping of g-C_3N_4 affected the crystallinity of the material, the crystalline phase is not changed. Except for the standard peaks corresponding to the standard spectra, the samples does not contain other impurity peaks or peaks of other compounds, which indicate that the purity of samples is high. However, compared with the XRD patterns of pure SnO_2, the diffraction peaks of g-C_3N_4 cannot be observed in the XRD patterns of SnO_2/g-C_3N_4 composites. This might be due to the relatively small amount of g-C_3N_4. Another reason could be that the peak of g-C_3N_4 at around 27.5° overlaps with the peak of SnO_2 at around 26.6°.

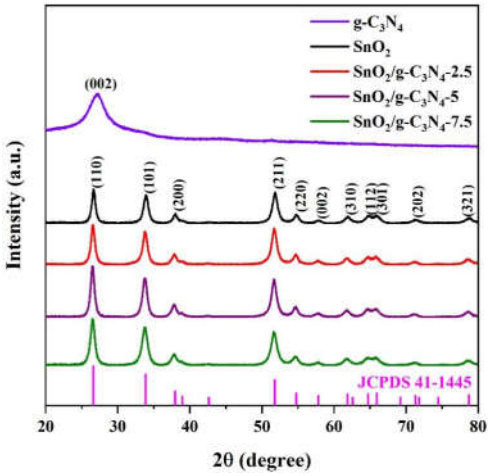

Figure 1. XRD patterns of g-C_3N_4, SnO_2 and SnO_2/g-C_3N_4 composites.

SEM studies

The morphology and microscopic surface morphology of g-C_3N_4, SnO_2 and SnO_2/g-C_3N_4 composites were observed using SEM. From Figure 2(a, e), it can be observed that the 3D flower-like hierarchical structure of pure SnO_2 assembled from nanosheets, with a nanosheet thickness of approximately 5nm and a clustered morphology. Compared with pure SnO_2, SnO_2/g-C_3N_4-2.5 in Figure 2(b, f) gradually shows a flower-like morphology with nanosheet dispersion, which may be due to the fact that g-C_3N_4 plays a template-oriented role during the material synthesis, which has no adverse effect on the growth of SnO_2. Figure 2(c, g), with the amount of g-C_3N_4 increased further, SnO_2/g-C_3N_4-5 shows a unique flower-like graded structure assembled by uniformly sized and dispersed nanosheets, which can be clearly seen that the nanosheets are very thin with a thickness of about 20 nm, and many uniformly sized pores are also distributed on the nanosheets, which provides more reaction sites for gas adsorption and is beneficial to improving the gas-sensitive performance. When the content of g-C_3N_4 is 7.5 wt%, a large area of the nanosheets appears broken agglomeration and aggregates along with the formation of nanoparticles, as in Figure 2 (d, h). Therefore, adding appropriate amount of g-C_3N_4 results in better homogeneity and dispersion of the flower-like structure. However, because of the low content of g-C_3N_4, g-C_3N_4 nanosheets cannot be observed in the SnO_2/g-C_3N_4 microscopic surface morphology.

As illustrated in Figure 3, to further demonstrate the SnO_2/g-C_3N_4 composites have been successfully synthesized, the chemical composition of the SnO_2/g-C_3N_4-5 composites are analyzed by EDS, the result shows both Sn, O, C, and N elements exist, which means the composites have been successfully synthesized.

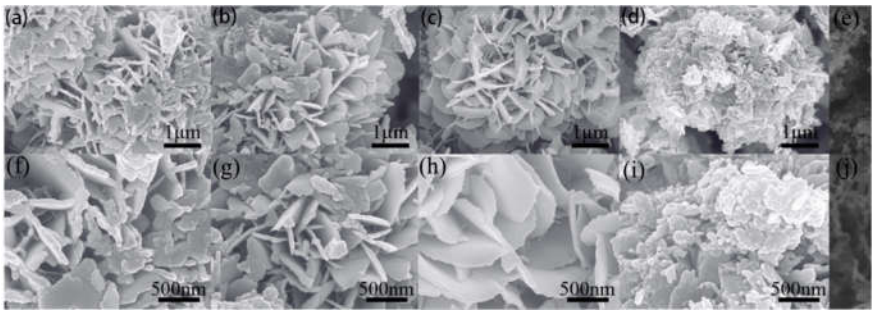

Figure 2. SEM images of (a, f) pure SnO_2, (b, g) SnO_2/g-C_3N_4-2.5, (c, h) SnO_2/g-C_3N_4-5, (d, i) SnO_2/g-C_3N_4-7.5 and (e, f) g-C_3N_4

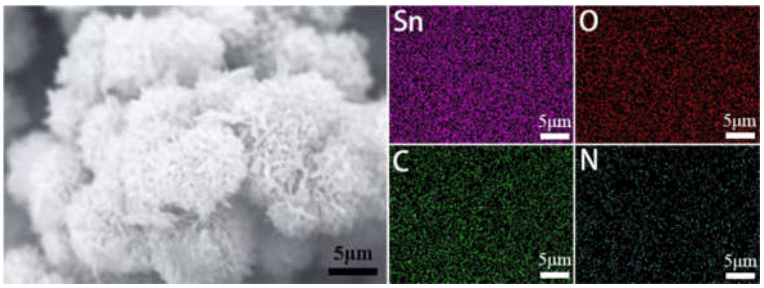

Figure 3. EDS spectra of SnO_2/g-C_3N_4-5 samples for elemental analysis of Sn, O, C and N.

Nitrogen adsorption and desorption analysis

Figure 4 presents the N_2 adsorption-desorption isotherms and pore size distribution curves of g-C_3N_4, SnO_2 and SnO_2/g-C_3N_4-5. As shown in Figure 4(a) and (c), the N_2 adsorption-desorption of the three samples display typical type IV curves with H3-type hysteresis lines according to IUPAC, which indicates mesoporous structure is present in the sample. The BET calculations yielded the specific surface areas of the g-C_3N_4, SnO_2 and SnO_2/g-C_3N_4-5 samples, which were 187.8 m^2/g, 28.81 m^2/g and 129.98 m^2/g. The additional g-C_3N_4 increased the specific surface area of the composites, and the large specific surface provided more reaction sites for gas adsorption. In addition, the change in specific surface area is part of the complex phase transition and is accompanied by the growth of nanostructures with different morphologies. Figure 4 (b) and (d) show the pore size distribution curves of the three samples. It can be observed that all samples show relatively small pore sizes, the pore sizes of g-C_3N_4 are in the range of 3-7.5 nm, the pore sizes of SnO_2 and SnO_2/g-C_3N_4-5 are mainly in the range of 2-6 nm. Such a porous structure can promote gas transport and adsorption and improve gas-sensitive performance.

Gas-sensitive performance

One of the most critical factors for gas sensors is the temperature property. Because of the resistance of a metal oxide semiconductor varies with the adsorption-desorption behavior of the gas and the temperature will directly affect the adsorption and desorption behavior of the gas molecules on the material. As a result, the metal oxide semiconductor's response to gases will be varied with temperature.

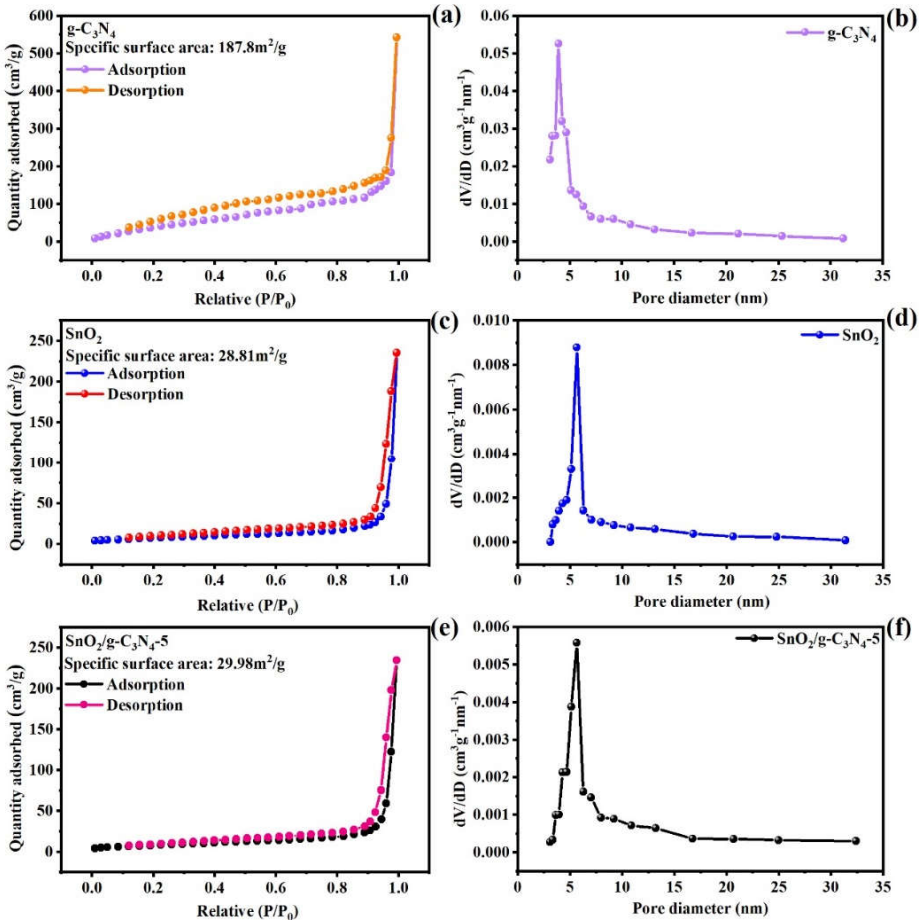

Figure 4. (a) N_2 adsorption-desorption isotherms and (b) pore size distribution curves for g-C_3N_4; SnO_2 and SnO_2/g-C_3N_4-5 (c) N_2 adsorption-desorption isotherms and (d) pore size distribution curves for g-C_3N_4; SnO_2 and SnO_2/g-C_3N_4-5.

The gas-sensitive response of the sensor at various temperatures for an ethanol concentration of 100 ppm was examined to ascertain the ideal operating temperature of the sensor in order to explore the material's optimal operating temperature. As the operating temperature rises, all curves display the same pattern of "increasing, max, and decreasing," as seen in Figure 5. Due to the chemisorbed oxygen species obtaining the energy necessary to react with the ethanol gas molecules at 200 °C, the response values of the SnO_2 and SnO_2/g-C_3N_4 sensors achieve their maximum at this temperature. The resistance is dramatically changed as a result of this reaction, which essentially takes place on the metal oxide semiconductor's surface. Varying g-C_3N_4 doping amounts directly affects the gas-sensitive performance of the material to ethanol. At low level, the gas response is increased with increasing g-C_3N_4 doping due to the high conductivity of g-C_3N_4, but it decreases when the doping amount is too large. When the g-C_3N_4 content in the composites exceed a certain value, the specific surface areas of the composites decrease and there are reduced active sites for adsorption oxygen and ethanol gas, leading to the degradation of gas

sensing properties. In addition, the response value of the SnO_2/g-C_3N_4-5 sensor is much higher than that of the pure SnO_2 sensor. At 200°C, the response of the SnO_2/g-C_3N_4 sensor to 100 ppm ethanol was 18.88, which was 2.09 times higher than the response of the pure SnO_2 sensor. The g-C_3N_4 reduces the bandgap width of SnO_2. The reduction of the bandgap width of the sample reduces the energy required for electrons to transition from the valence band to the conduction band, therefore, the operating temperature of the material is reduced. All subsequent tests were performed at 200 °C.

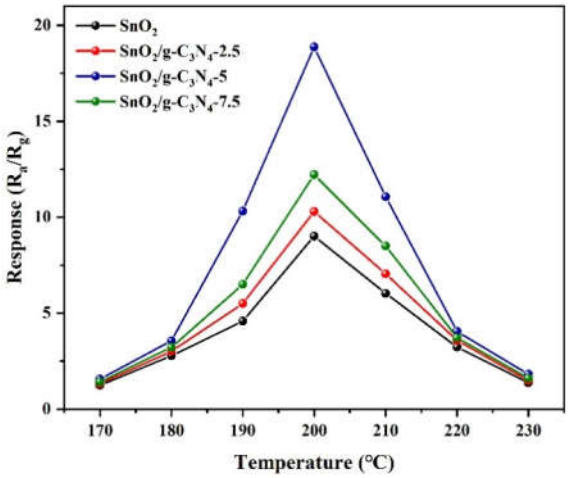

Figure 5. Response of SnO_2 and SnO_2/g-C_3N_4 sensors to 100 ppm ethanol at different operating temperatures.

Figure 6(a) displays the dynamic response-recovery curves of the pure SnO_2 and SnO_2/g-C_3N_4-5 sensors for different concentrations of ethanol, each with a response-recovery period of 150 s, a response interval of 75 s, and a recovery interval of 75 s. It can be observed that the responses amplitude of both sensors increase significantly once they are exposed to ethanol gas and then return to their initial values, which indicates that they have good response-recovery characteristics for ethanol gas. As shown in Figure 6(b), the concentration-dependent response of the sensors at 200 °C is plotted to show the relationship between the response and the gas concentration, and the response values of both sensors increase with increasing ethanol concentration in the range of 10-500 ppm. The response of the SnO_2/g-C_3N_4-5 sensor to the same concentration of ethanol was significantly higher than that of the pure SnO_2 sensor, and the gas-sensitive performance of the composite material is greatly improved, as expected from the composite. In Figure 6(c), the response of SnO_2/g-C_3N_4-5 to 100-500 ppm ethanol increases linearly with the relational equation and correlation coefficient of $y = 5.80275+0.1288$ and $R^2 = 0.96219$, respectively, which implies that the prepared SnO_2/g-C_3N_4-5 sensor has great potential to detect ethanol. The response-recovery time is one of the important factors to affect the response of the affected gas sensor. From the curve in Figure 6(d), it can be seen that the response of the SnO_2/g-C_3N_4-5 sensor increases and decreases rapidly when exposed to ethanol and separated from ethanol, respectively. The response and recovery time are 2 s and 13 s. This good response-recovery can be attributed to the unique porous, flower-like, graded structure of SnO_2/g-C_3N_4, which not only gives it a high specific surface area but also accelerates the adsorption of ethanol molecules. The high electrical conductivity of g-C_3N_4 also promotes the adsorption of gas molecules on the SnO_2 surface, thus shortening the response time.

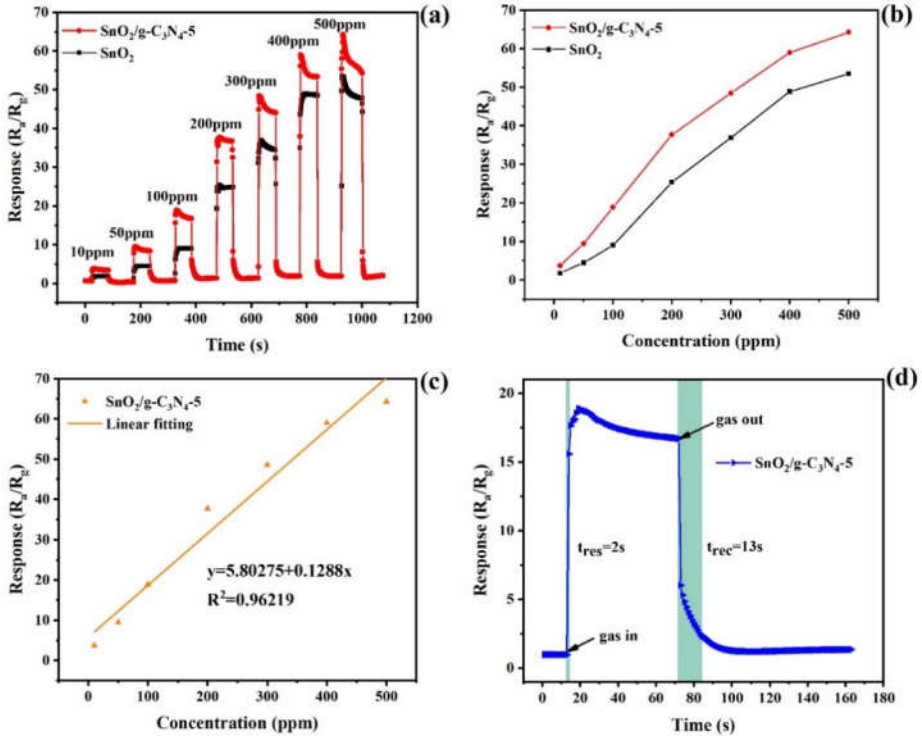

Figure 6. (a) Dynamic response-recovery curves and (b) curve relationships of SnO_2 and SnO_2/g-C_3N_4-5 sensors for different ethanol concentrations at 200 °C; (c) linear fit curves of SnO_2/g-C_3N_4-5 sensors for different ethanol concentrations; (d) response-recovery curves of SnO_2/g-C_3N_4-5 sensors for 100 ppm ethanol at 200 °C Time

Both repeatability and stability are key factors affecting gas-sensitive performance. Figure 7(a) displays the SnO_2/g-C_3N_4-5 sensor's repeatability at 200 °C for 100 ppm ethanol. The curve depicts that after four response cycles, the response value stays nearly constant at 18.88. The developed SnO_2/g-C_3N_4-5 sensor has good repeatability for sensing ethanol gas, it can be said. The persistent response of the SnO_2/g-C_3N_4-5 sensor to 100 ppm is evaluated for 30 days to confirm the stability of the sensor, as shown in Figure 7(b), the response value to 100 ppm ethanol keeps about 18.88 at 200 °C. Therefore, SnO_2/g-C_3N_4 sensors have excellent stability.

Another important element in determining a gas sensor's level of quality is selectivity. Figure 8 shows the results of selectivity tests for six different gases using pure SnO_2 and SnO_2 /g-C_3N_4-5 sensors (including methanol, acetone, ethanol, xylene, trimethylamine and formaldehyde). As can be shown, the SnO_2 /g-C_3N_4-5 sensor has greater ethanol selectivity at 200 °C than pure SnO_2. The stronger reaction to ethanol might be because the hydroxyl group (-OH) is more readily oxidized at the ideal operating temperature, whereas ethanol is more likely to lose electrons via the redox process of adsorbed oxygen. The ethanol sensing performance of the prepared SnO_2/g-C_3N_4-5 sample is compared with other SnO_2-based ethanol sensors reported in the literature. As shown in Table 1, the prepared SnO_2/g-C_3N_4-5 nanomaterial exhibits a higher response at lower operating temperature, which indicate that they are the ideal candidates for ethanol sensors.

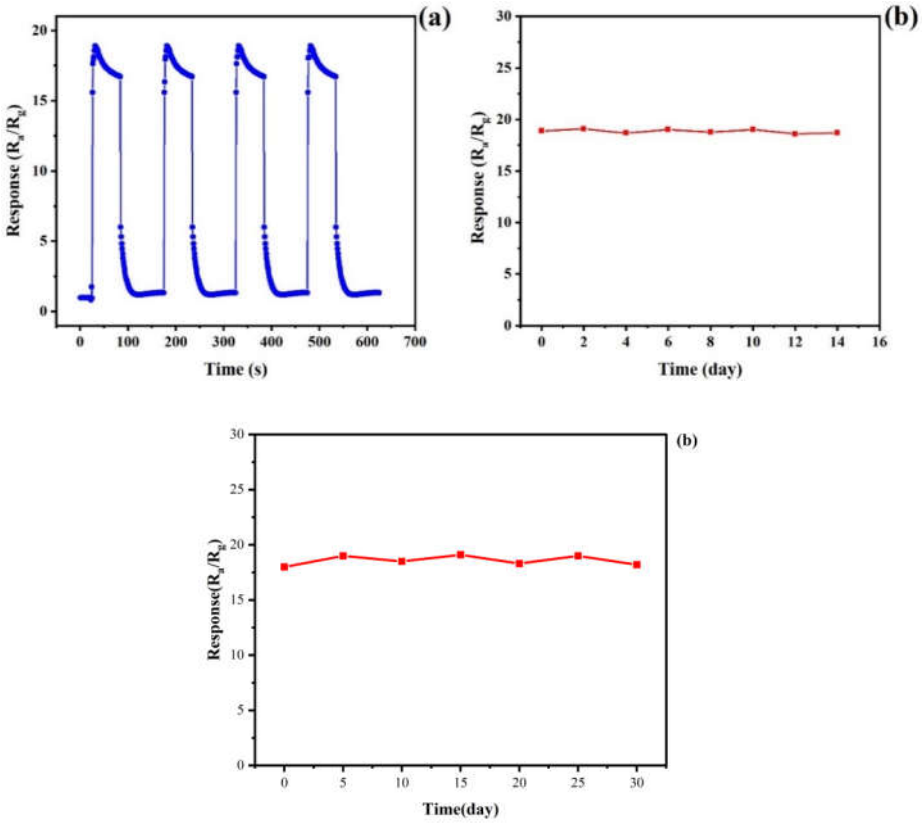

Figure 7. Repeatability (a) and stability (b) of SnO_2/g-C_3N_4-5 sensor at 200 °C for 100 ppm ethanol.

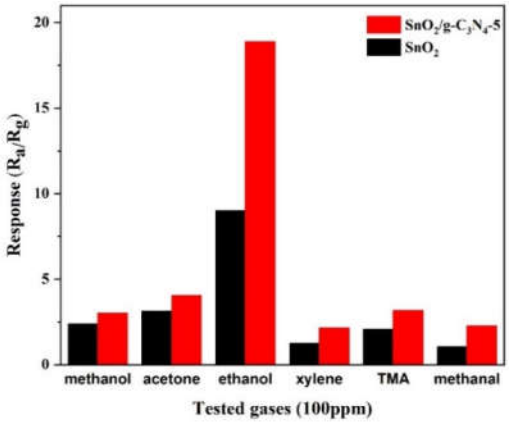

Figure 8. Histogram of response of SnO_2 and SnO_2/g-C_3N_4-5 sensors at 200 °C for different gases at 100 ppm.

Table 1. Comparison of the gas-sensitive performance of SnO_2-based ethanol sensors based on different morphologies.

Gas-sensitive materials	Operating temperature (°C)	Ethanol (ppm)	Response (R_a/R_g)	Ref.
SnO_2/CuO nanoparticles	320	100	8.0	[19]
SnO_2 hollow sphere	350	100	10.5	[20]
SnO_2/ZnO graded nano structure	400	100	6.2	[21]
Au@SnO_2 graded hollow microspheres	240	100	23.93	[22]
Flower-like grading structure SnO_2/g-C_3N_4	200	100	18.88	Present work

Gas-sensitive mechanism

The mechanism of metal oxide semiconductor gas sensors is related to the space charge layer theory. For a single SnO_2 sensitive material, the gas-sensitive mechanism can be described by the space charge layer model, and the resistance change of the sensitive material is related to the adsorption and desorption of the test gas on the material surface. Generally, the doping of 2D g-C_3N_4 in SnO_2/g-C_3N_4 composites plays an important role in preventing the aggregation of SnO_2 particles, that promote the self-assembly of SnO_2 nanoparticles into a 3D flower-like hierarchical structure. The high specific surface area of the composite sample is due to the heterojunction of g-C_3N_4 nanosheets and SnO_2 spheres, which facilitates the reaction of gases on the sensing layer surface, especially the adsorption and diffusion processes of ethanol molecules. 2D g-C_3N_4 nanosheets can provide more active sites to adsorb O_2 and ethanol molecules. The improved gas-sensitive performance of the SnO_2/g-C_3N_4 composite sensor for ethanol is attributed to the heterojunction in the interfacial region between g-C_3N_4 and SnO_2. It is well known that SnO_2 and g-C_3N_4 are n-type semiconductors with band gaps of 3.6 eV and 2.7 eV. The conduction band energy level of g-C_3N_4 is lower than that of SnO_2. Coupling SnO_2 with g-C_3N_4 to construct the heterojunction structure could be an efficient way to lead electrons flow from the conduction band of g-C_3N_4 to that of SnO_2, which results in an increase in the width of the potential barrier and results in the high resistance of the sensor (Ra). As a result, a higher response due to the increased conductivity of the heterojunction structure. As shown in Fig. 9, when the sensor is exposed to air, oxygen molecules will be adsorbed on the surface of SnO_2 and the electrons are tapped from the conduction band of SnO_2. The oxygen molecules are ionized into O^{2-}, O^- and O_2^-, as in the following Eq. (1-4):

$$O_2(gas) \rightarrow O_2(ads) \quad (1)$$

$$O_2(ads) + e^- \rightarrow O_2^-(ads)\ (100°C<T) \quad (2)$$

$$O_2^-(ads) + e^- \rightarrow 2O^-(ads)\ (100°C<T<300°C) \quad (3)$$

$$O^-(ads) + e^- \rightarrow O^{2-}(ads)\ (300°C<T) \quad (4)$$

The formation of the electron-withdrawal layer leads to an increase in the resistance of the composite sensor. Nevertheless, when the sensor is exposed to ethanol gas, the ethanol molecules react with the oxygen ions absorbed on the sensor surface. The ethanol molecules react with the adsorbed oxygen ions to form carbon dioxide and water. As follows:

$$C_2H_5OH(gas) + 6O^- = 2CO_2 + 3H_2O + 6e^- \quad (5)$$

Consequently, the captured electrons are released back into the depletion layer of the sensing system which leads to a reduction in the resistance of the composite sensor.

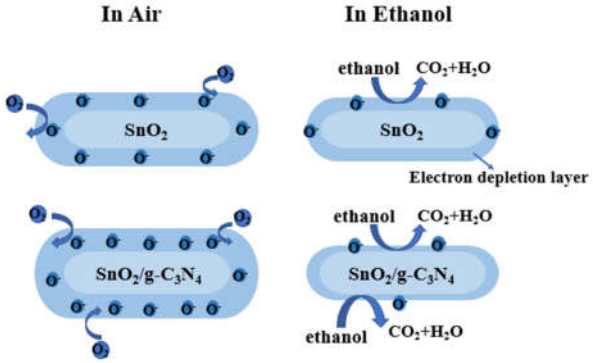

Figure 9. The schematic diagram of acetone sensing mechanism for SnO_2/g-C_3N_4 based sensor.

CONCLUSION

In this paper, SnO_2/g-C_3N_4 composites with the flower-like grading structure were prepared by hydrothermal process and which were assembled by irregular nanosheets with a thickness of 20-40 nm. The gas sensing study indicates that the response of SnO_2/g-C_3N_4 to 100 ppm ethanol at 200 °C is 18.8, with response and recovery time of 2 s and 13 s, respectively. It shows excellent selectivity for ethanol gas compared with other gases and also exhibits good repeatability and stability. The excellent gas-sensitive performance is attributed to the flower-like graded structure, the n-n heterojunction, and the interaction between SnO_2 and g-C_3N_4. This experiment provides new ideas and insights for the design and fabrication of MOS sensors with flower-like hierarchical structures.

ACKNOWLEDGEMENTS

This work was supported by the Science Research Project of Education Department, Jilin Province (Grant No. JJKH20230322KJ).

REFERENCES

1. Hoa, L.T.; Cuong, N.D.; Hoa, T.T.; Khieu, D.Q.; Long, H.T.; Quang, D.T.; Hoa, N.D.; Hieu, N.V. Synthesis, characterization, and comparative gas sensing properties of tin dioxide nanoflowers and porous nanospheres. *Ceram. Int.* **2015**, 41, 14819-14825.
2. Meng, F.L.; Liao, Z.J.; Xing, C.Y.; Yuan, Z.Y.; Zhang, R.Z.; Zhu, H.M.; Li,J. Preparation of SnO_2/SiO_2 nanocomposites by sol-gel method for enhancing the gas sensing performance to triethylamine. *J. Alloy. Compd.* **2022**, 893, 162189-162195.
3. Zhen, Y.X.; Song, B.Y.; Liu, W.X.; Ye, J.X.; Zhang, X.F.; Deng, Z.P.; Huo, L.H.; Gao, S. Ultra-high response and low temperature NO_2 sensor based on mesoporous SnO_2 hierarchical microtubes synthesized by biotemplating process. *Sens. Actuators B Chem.* **2022**, 363, 131852-131862.
4. Kou, X.Y.; Meng, F.Q.; Chen, K.; Wang, T.S.; Sun, P.; Liu, F.M.; Xu, Y.; Sun, Y.F.; Liu, F. M.; Shimanoe, K.; Lu, G.Y. High-performance acetone gas sensor based on Ru-doped SnO_2 nanofibers. *Sens. Actuators B Chem.* **2020**, 320, 128292-128299.
5. Akhir, M.A.M.; Rezan, S.A.; Mohamed, K.; Arafat, M.M.; Haseeb, A.S.M.A.; Lee, H.L.

Synthesis of SnO_2 nanoparticles via hydrothermal method and their gas sensing applications for ethylene detection. *Mater. Today: Proceedings* **2019**, 17, 810-819.
6. Liu, L.Y.; Zhou, P.; Su, X.Z.; Liu, Y.H.; Sun, Y.H.; Yang, H.B.; Fu, H.Y.; Qu, X.L.; Liu, S. T.; Zheng, S.R. Synergistic Ni single atoms and oxygen vacancies on SnO_2 nanorods toward promoting SO_2 gas sensing. *Sens. Actuators B Chem.* **2022**, 351, 130983-130993.
7. Kim, J. H.; Park, H.; Mirzaei, A.; Hahm, M. G.; Ahn, S.; Halik, M.; Park, C.; Kim, S. S. How femtosecond laser irradiation can affect the gas sensing behavior of SnO_2 nanowires toward reducing and oxidizing gases. *Sens. Actuators B Chem.* **2021**, 342(1), 130036-130045.
8. Yang, C.Y.; Liu, B.H.; Yang, Y.; Wang, T.T.; Wang, T.Q.; Yu, H.; Dong, X.T. Indium element-induced oxygen vacancies and polycrystalline structure enabled SnO_2 nanofibers for highly sensitive detection of NO_x. *Sens. Actuators B Chem.* **2022**, 362, 131754-131763.
9. Huang, J.R.; Meng, C.Y.; Wang, H.; Ren, H.B.; Lu, X.J.; Joo, S.W. Preparation of cross-linked porous SnO_2 nanosheets using three-dimensional reduced graphene oxide as a template and their gas sensing property. *J. Alloy. Compd.* **2022**, 910, 164763-164771.
10. Wang, Y.Y.; Na, H.B.; Zhang, M.; Deng, Z.P.; Huo, L.H.; Gao, S. Coca-Cola solvothermal synthesis of mesoporous SnO_2 blooming flower-like architecture assembled from single crystal nanorods and its gas sensing properties. *Powder Technol*. **2020**, 375, 463-471.
11. Xu, L.N.; Zeng, W.; Li, Y.Q. Synthesis of morphology and size-controllable SnO_2 hierarchical structures and their gas-sensing performance. *Appl. Surf. Sci.* **2018**, 457, 1064-1071.
12. Wang, Q.; Yao, N.; An, D.M.; Li, Y.; Zou, Y.L.; Lian, X.X.; Tong, X.Q. Enhanced gas sensing properties of hierarchical SnO_2 nanoflower assembled from nanorods via a one-pot template-free hydrothermal method. *Ceram. Int.* **2016**, 42, 15889-15896.
13. Hu, J.C.; Wang, H.P.; Chen, M.P.; Zhang, Y.M.; Zhao, X.B.; Zhang, D. M.; Lu, Q. J.; Zhang, J.; Liu, Q. J. Constructing hierarchical SnO_2 nanoflowers for enhanced formaldehyde sensing performances. *Mater. Lett.* **2020**, 263, 126843-126845.
14. Zhang, J.Y.; Zhang, B.W.; Yao, S.J.; Li, H.Y.; Chen, C.; Bala, H.; Zhang, Z.Y. Improved triethylamine sensing properties of fish-scale-like porous SnO_2 nanosheets by decorating with Ag nanoparticles. *J. Materiomics* **2022**, 8, 518-525.
15. Fan, H.Q.; Zheng, X.K.; Shen, Q.; Wang, W.J.; Dong, W.Q. Hydrothermal synthesis and their ethanol gas sensing performance of 3-dimensional hierarchical nano Pt/SnO_2. *J. Alloy. Compd.* **2022**, 909, 164693-164700.
16. Xue, D.P.; Wang, Y.; Cao, J.L.; Zhang, Z.Y. Hydrothermal synthesis of CeO_2-SnO_2 nanoflowers for improving triethylamine gas sensing property. *J. Nanomater.* **2018**, 1025-1035.
17. Liu, M.; Song, P.; Yang, Z.X.; Wang, Q. Hierarchical assembly of SnO_2 nanorod on spindle-like α-Fe_2O_3 for enhanced acetone gas-sensing performance. *Ceram. Int*. **2021**, 47, 121181-12188.
18. Karthik, P.; Gowthaman, P.; Venkatachalam, M.; Saroja, M. Design and fabrication of g-C_3N_4 nanosheets decorated TiO_2 hybrid sensor films for improved performance towards CO_2 gas. *Inorg. Chem. Commun*. **2020**, 119, 108060.
19. Zhang, J.L.; Ma, S.Y.; Wang, B.J.; Pei, S.T. Hydrothermal synthesis of SnO_2-CuO composite nanoparticles as a fast-response ethanol gas sensor. *J. Alloy. Compd.* **2021**, 886, 161299-161308.
20. Wang, B.; Sun, L.; Wang, Y.D. Template-free synthesis of nanosheets-assembled SnO_2 hollow spheres for enhanced ethanol gas sensing. *Mater. Lett*. **2018**, 218, 290-294.
21. Khoang, N.D.;Trung, D.D.; Duy, N.V.; Hoa, N.D.; Hieu, N.V. Design of SnO_2/ZnO hierarchical nanostructures for enhanced ethanol gas-sensing performance. *Sens. Actuators B Chem.* **2012**, 174, 594-601.
22. Liu, Y.M.; Li, X.;Wang, Y.L.; Li, X.W.; Cheng, P.F.; Zhao, Y.; Dang, F.; Zhang, Y.Q. Hydrothermal synthesis of Au@SnO_2 hierarchical hollow microspheres for ethanol detection. *Sens. Actuators B Chem.* **2020**, 319, 128299-128308.